Turkish Computational and Theoretical Chemistry

Turkish Comp Theo Chem (TC&TC)

Volume(Issue): 9(2) – Year: 2025 – Pages: 8-18

e-ISSN: 2602-3237

https://doi.org/10.33435/tcandtc.1502035

Received: 16.06.2024 ***Accepted***: 13.08.2024 *Research Article*

SARS-COV-2 Inhibitors from Azadirachta indica Leaves: Chemical Composition, Molecular Docking and Quantum Chemical Studies

Ifeanyi Edozie Otuokere[a,1], Chinedum Ifeanyi Nwankwo[b], Onuchi Marygem Mac-kalunta[a], Julian Ibeji Iheanyichukwu[a], Chidiebere Onwukwe Agu[a]

[a]Department of Chemistry, Michael Okpara University of Agriculture, Nigeria
[b]Department of Biochemistry, Michael Okpara University of Agriculture, Nigeria

Abstract: Since late 2019, the highly transmissible and virulent coronavirus SARS-CoV-2 has been the source of a pandemic called COVID-19. The public's health and safety were at risk because of this pandemic. The aim of this research is to identify phytoactive compounds derived from Azadirachta indica that may be employed as a possible SARS-CoV-2 inhibitor. Twenty chemicals were found in the leaves of A. indica by GC-MS analysis. Molecular docking indicated that the phytocompounds had good binding energies. The compound with the best hit was 1,6,10,14,18,22-Tetracosahexaen-3-ol,2,6,10,15,19,23-hexamethyl (compound 14) with a binding affinity of -4.9 Kcal/mol. The compound 14, which was identified as the top-hit compound, underwent geometry optimisation. Subsequently, the electronic properties such as HOMO, LUMO, and electrostatic potential (ESP) mapping electron density surface, bond lengths, bond angles, ZDO charges, Mulliken atomic charges and NMR were simulated. This was done using the PM3 (NDDO) Quantum Mechanical Parameterization approach, which is based on Hartree-Fock calculation, in the ArgusLab 4.0.1 software. The best conformation was determined to be -102.39 au, which is the minimum potential energy calculated by the geometry convergence function. The molecular geometry was obtained by achieving convergence. All of the obtained results lead us to delineate the active sites with charged groups to interact with the receptors. These kinds of investigations are significant for drug-receptor interactions.

Keywords: *Azadirachta indica*, GC-MS, SARS-CoV-2, docking, *in silico*

A. Indica

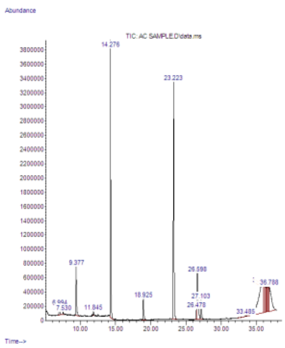

Gas chromatogram

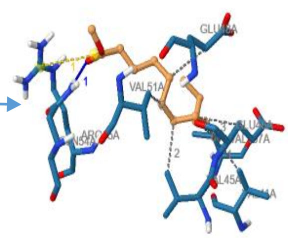

3D visualization

1. Introduction

A new coronavirus known as SARS-CoV-2 surfaced in Wuhan, China, in 2019, resulting in an unusual viral pneumonia outbreak. The coronavirus disease, which is extremely contagious and sometimes referred to as COVID-19, has been

[1] Corresponding Authors

e-mail: ifeanyiotuokere@gmail.com & ifeanyiotuokered@mouau.edu.ng

spreading swiftly. It has significantly outperformed SARS and MERS in terms of the quantity of ill patients as well as the geographic range of the epidemic regions. The current COVID-19 outbreak, which exhibits age-specific clinical signs, poses a serious risk to public health. In one study, individuals over sixty years old had increased bilateral extralobe sores, inflammatory indicators, and blood urea nitrogen levels. Individuals over 60 had a longer illness course and a higher risk of developing respiratory failure [1]. A survey found that there have been 72,314 confirmed cases in China, with individuals ages 30 to 79 making up the majority of cases (87%). There were no deaths among children aged nine and below. In the case-fatality rate (CFR), the age range of 70 to 79 years is 8.0 percent, whereas the age range of 80 years and above is 14.8 percent. For people with different concomitant diseases such as cancer, diabetes, heart disease, hypertension, and chronic lung disease, the CFR is 10.5, 7.3, 6.3, 6.0, and 5.6 percent, respectively. According to these findings, comorbid disorders significantly increase the probability of death for COVID-19 carriers compared to those without underlying medical conditions [2]. Guan and co-workers [3] reported that COVID-19 confirmed 1,099 cases of patients with severe illnesses. The majority of the 1,391 infected children, with a median age of 6.7 years, have less severe symptoms than adults [4]. COVID-19 increases the risk of death in patients over 65, particularly those with AIDS and other comorbidities [5–8].

Plant products-also called natural products-inhibit bacterial growth, increase antioxidant activity, and modify genetic expression, all of which are crucial for disease prevention and treatment. There is still much to learn about the therapeutic utility of a number of plants in managing disease since they have few adverse effects and are inexpensive. It is commonly known that allopathic drugs are expensive and detrimental to healthy tissues and biological processes. Many nations have found great success in managing diseases with a variety of medicines made from plant substances. It is often known that a large number of medications with pharmacological potency originate from natural resources, including therapeutic plants [9, 10]. *A. indica* is native to tropical and semitropical regions, including Nigeria, Ghana, India, and Nepal. It belongs to the Meliaceae family. It is a quick growing tree with a trunk diameter of 4-5 feet and a height of 20–23 metres. Each leaflet in the complex, imparipinnate leaves ranges from five to fifteen. It produces green drupes. Between June and August, the drupe becomes golden yellow in colour. Neem components are used in Ayurveda, homoeopathy, and modern medicine [11,12]. Among the components of *A. indica* are limonoids, nimbin, nimbidin, and nimbolide. These compounds function by altering several genetic pathways and other mechanisms to treat diseases. Quercetin and ß-sitosterol, two polyphenolic flavonoids with antifungal and antibacterial qualities, were the first to be extracted from fresh neem leaves [13]. There have been reports of *A. indica's* antibacterial, antifungal, and anti-inflammatory qualities [14–16]. Researchers have confirmed that *A. indica* possesses medicinal properties [17–20]. Certain parts of the *A. indica* plant have the ability to suppress microbial growth and cell wall breakdown, which has an antibacterial effect. The primary ingredient in seeds that has both toxic and insect-repelling properties is azadirachtin, a complex limonoid tetranortriterpenoid [18]. The antibacterial potency of *A. indica* ethanol leaf extract against *S. aureus* has been reported [21].

Researchers have used GC-MS to explore phytocompounds in plants [22–36]. Few reports exist on the leaves of *A. indica*. The bioactive chemicals found in *A. indica* leaves have not been fully reported. The GC-MS characterization, molecular docking and quantum chemical studies of *A. indica*. leaves bioactive phytocompounds have not been documented. Based on the information available to us, this is the first study to use *in silico* molecular docking, GC-MS and quantum chemical studies on the leaves of *A. indica*. Thus, the purpose of this work is to identify putative SARS-CoV-2 inhibitors in *A. indica* leaves.

2. Computational Method

2.1. Extraction

The harvest of *A. indica* leaves took place at Umudike, Abia State, Nigeria, on March 23, 2022, between 7.00 and 7.30 a.m. The forestry department at Michael Okpara University of Agriculture, Umudike (MOUAU) identified the plant and gave it a herbarium number. The leaves were grated. The weighed and grated leaves were allowed to air dry for four weeks. It was 1.2 kg in weight. For a duration of 72 hours, the material was macerated in three litres of 99.8% methanol, after which it was decanted, filtered, and concentrated.

2.2. GC-MS analysis

The analysis was carried out using a gas chromatograph interfaced to a mass spectrometer apparatus SCHIMADZU (GCMS-QP2010 PLUS). The working conditions described by Otuokere *et al.* [32] were followed.

2.3. Identification of phytochemical Components of the GC-MS

Compounds were identified by cross-referencing mass spectrum data and retention indices with the NIST Mass Spectroscopy Library and the Wiley Registry of Mass Spectral Data, 8th edition. The identification was further confirmed by calculating retention indices (RI) in relation to a homologous sequence of n-alkanes under the same experimental conditions and comparing the results with those reported in the literature.

2.4. Preparation of SARS-CoV-2 protein and identified compounds

The SARS-CoV-2 protein (PDB ID: 7K3N) was obtained by using the RCSB Protein Databank. The H_2O molecules were extracted using the ArgusLab 4.0.1 programme [37].

2.5. Molecular docking study

Docking was performed using the PyRx Virtual Screening Tool [38].

2.6. Quantum Chemical Studies

The compound 14, which was identified as the top-hit compound, underwent geometry optimisation. Subsequently, the electronic properties, including HOMO, LUMO, electrostatic potential (ESP) mapping electron density surface, geometric optimization, bond lengths and angles were simulated. This was done using the AM1 (NDDO) Quantum Mechanical Parameterization approach, which is based on Hartree-Fock calculation, in the ArgusLab 4.0.1 software. The molecular geometry was obtained by achieving convergence in ArgusLab. The programme thereafter computed the energy until reaching the maximum number of cycles, ensuring the molecule's convergence.

3. Results and discussion

3.1. GC-MS Analysis

A total of 20 bioactive peaks were visible in the GC chromatogram of the methanol extract of *A. indica* leaves. Figure 1 shows the GC chromatogram of the *A. indica* leaf methanol extract. Twenty phytocompounds were found in the GC chromatogram, according to the data (Table 1).

3.2. Molecular docking studies

The SAR-SCoV-2 protein was used to dock all phytocompounds. Table 1 shows the phytocompounds' docking results with 7K3N. The binding affinity of the docking process ranged from -3.7 to -4.9 Kcal/mol. This indicated that the compounds bound successfully to the receptor. The best hit compound was compound 14. Quantum chemical plots of hit compound is presented in Figure 2. The HOMO and the LUMO are collectively referred to as the FMO. The HOMO can be understood as an orbital that is nucleophilic or donates electrons, and it is directly linked to the ionization potential. On the other hand, the LUMO is an electrophilic orbital that accepts electrons and is associated with the electron affinity of the molecule [39]. The FMO analysis is particularly useful for understanding the charge transfer between the electron donor and electron acceptor groups in conjugated compounds [39]. Figures 2b and c illustrate the HOMO and LUMO plots of the hit compound. The molecule's electronic transport is determined by the energy gap between the HOMO and the LUMO. The hit compound exhibits an energy gap of -5.77 eV. In the HOMO-LUMO plot, the blue colour indicates the positive phase of the orbital, while the red colour indicates the negative phase of the orbital. Understanding the FMO theory enables us to gain insights into the chemical reactivity and stability of the molecule. Molecular stability is crucial in the design of biomedically significant drugs. The energy difference between the EHOMO and the ELUMO is referred to as the energy gap of the molecule. A narrower energy gap results in decreased stability and increased reactivity of the molecule, whereas a wider energy gap leads to a more stable and less reactive system [39].

The chemical reactive descriptors, such as ionization potential, electron affinity, chemical hardness (η), chemical potential (μ), softness (ξ), electrophilicity index (ω), and electronegativity (χ) of the molecule, are determined using EHOMO and ELUMO energies and are presented in Table 2, based on Koopman's theorem. Mapped surfaces of compound 14 were generated (Figure 2e). Mapped surfaces of compound 14 were generated (Figure 2e). These surfaces represent the mapping of one property onto a surface generated by another property. The colours represent the numerical values of the electron density at specific spots on the surface. The colour map is provided on the left side. The ESP was projected onto the electron density surface. The ESP-mapped density surface represents the geometry of the surface, while the value of the ESP on that surface determines the colours. The electric potential at a specific point in space is the potential energy experienced by a positive "test" charge. A negative ESP value indicates that the positive test charge is in a stable zone. In contrast, a positive ESP indicates a zone of relative instability for the positive test charge. Therefore, the density surface of compound 14, which was mapped using ESP, reveals the specific areas of the molecule that are more prone to nucleophilic or electrophilic attack. These surfaces are valuable for making qualitative assessments of chemical reactivity. ESP-mapped density surfaces of the hit compound provide a visual representation of the locations where the frontier electron density of the molecule is either highest or lowest compared to the nuclei. The prominent alkyl groups in the chemical are represented by a sizable red region, indicating an area of increased electron density. The red colour signifies the areas with the highest negativity in the ESP, where a positive test charge would have favourable interaction energy. The hydroxyl terminus of the molecule, indicated by the magenta colour, exhibits areas of comparatively unfavourable energy for the ESP.

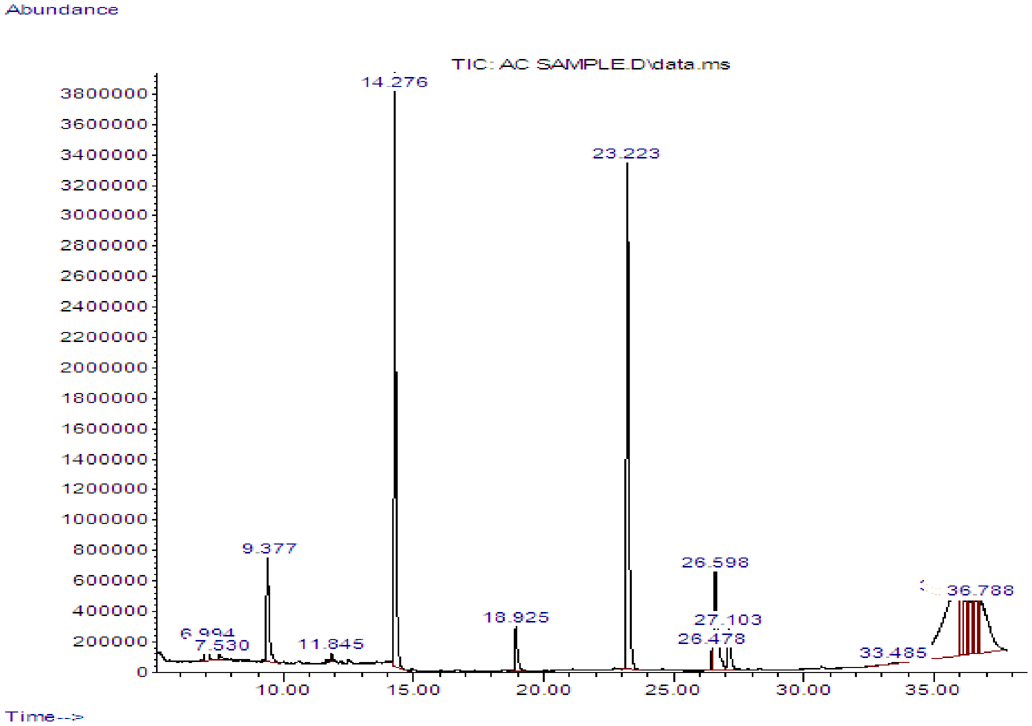

Figure 1. The chromatogram of GC of *A. indica* leaf methanol extract

Table 1. Phytocompounds present in the GC-MS of A. indica leaf methanol and their docking score

Comp No.	R.T (mins)	Mol. F. (g/mol)	Compound	Peak Area (%)	Mol.Weight	Binding Affinity (Kcal/mol)
1	6.99	172.26	Nonanoic acid, methyl ester	0.91	$C_{10}H_{20}O_2$	-3.7
2	7.53	150.21	D-Carvone	0.26	$C_{10}H_{14}O$	-4.7
3	9.37	186.29	Decanoic acid,methyl esther	4.69	$C_{11}H_{22}O_2$	-4.1
4	11.84	200.31	Undecanoic acid mehyl ester	0.23	$C_{12} H_{24}O_2$	-3.8

5	14.27	214.34	Dodecanoic acid,methyl ester	16.69	$C_{13}H_{26}O_2$	-4.2
6	18.92	242.39	Methyl tetradecanoate	1.95	$C_{15}H_{30}O_2$	-4.3
7	23.22	270.45	Hexadecanoic acid, methyl ester	22.25	$C_{17}H_{34}O_2$	-4.1
8	26.47	294.47	8,11-Octadecadienoic acid, methyl ester	0.66	$C_{19}H_{34}O_2$	-3.9
9	26.59	298.50	Methyl stearate	5.98	$C_{19}H_{38}O_2$	-4.3
10	27.10	296.48	9-Octadecenoic acid,methyl ester	2.02	$C_{19}H_{36}O_2$	-4.0
11	33.48	282.46	9-Octadecenoic acid	0.01	$C_{18}H_{34}O_2$	-4.2
12	35.77	282.46	Oleic acid	20.00	$C_{18}H_{34}O_2$	-4.0
13	36.04	282.46	Cis-vaccenic acid	3.29	$C_{18}H_{34}O_2$	-4.1
14	36.17	426.71	1,6,10,14,18,22-Tetracosahexaen-3-ol,2,6,10,15,19,23-hexamethyl	2.88	$C_{30}H_{50}O$	-4.9
15	36.28	282.46	Cis-13-octadecenoic acid	1.06	$C_{18}H_{34}O_2$	-4.1
16	36.41	338.56	Erucic acid	2.44	$C_{22}H_{42}O_2$	-4.0
17	36.50	238.40	cis-11-hexadecenal	1.80	$C_{16}H_{30}O$	-4.1
18	36.67	282.46	Trans-13-octadecenoic acid	3.95	$C_{18}H_{34}O_2$	-4.0
19	36.73	296.48	14-Octadecenoic acid,methyl ester	1.14	$C_{19}H_{36}O_2$	-4.1
20	36.78	254.40	Palmitoleic acid	7.78	$C_{16}H_{30}O_2$	-4.1

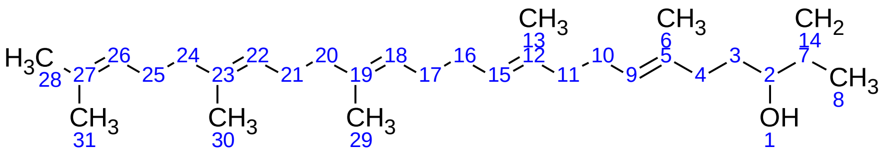

a) Structure of hit compound

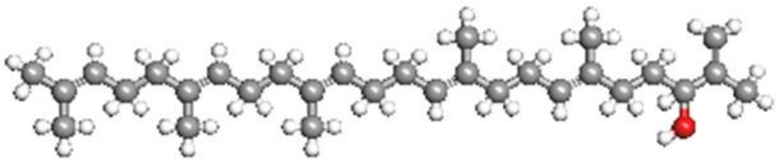

b) Optimized structure

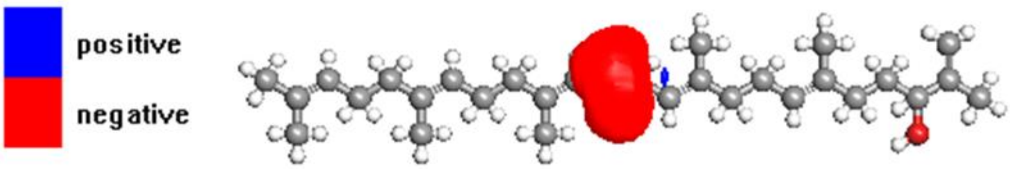

c) HOMO = -1.06 eV

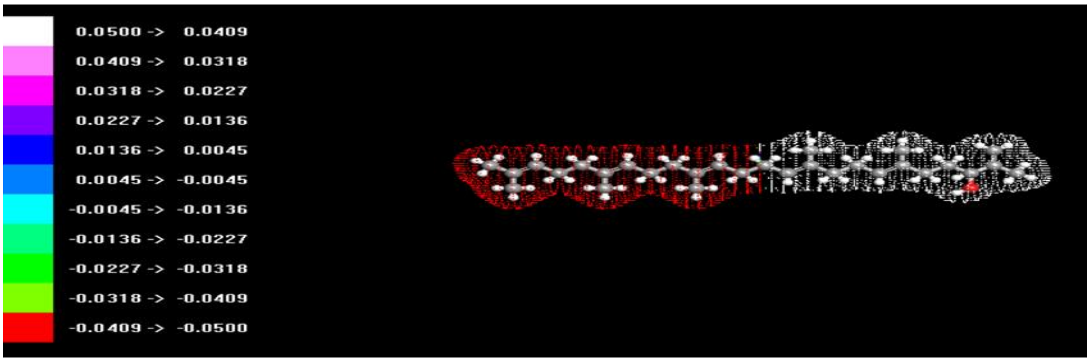

d) ESP mapping electron density surface

Figure 2. Quantum chemical plots of hit compound

Table 2. The chemical reactive descriptors of the hit Compound

Parameters	Values (eV)
E_{HOMO}	-1.06
E_{LUMO}	4.71
$E_{HOMO - ELUMO}$	-5.77
Ionization potential [$I = -E_{HOMO}$]	1.06
Electron affinity [$A = - E_{LUMO}$]	-4.71
Chemical hardness [$\eta = (I - A)/2$]	2.89
Electronegativity [$\mu = - (I + A)/2$]	1.83
Softness [$\xi = 1/2\eta$]	0.17
Electrophilicity index [$\chi = \mu^2/2\eta$]	0.58

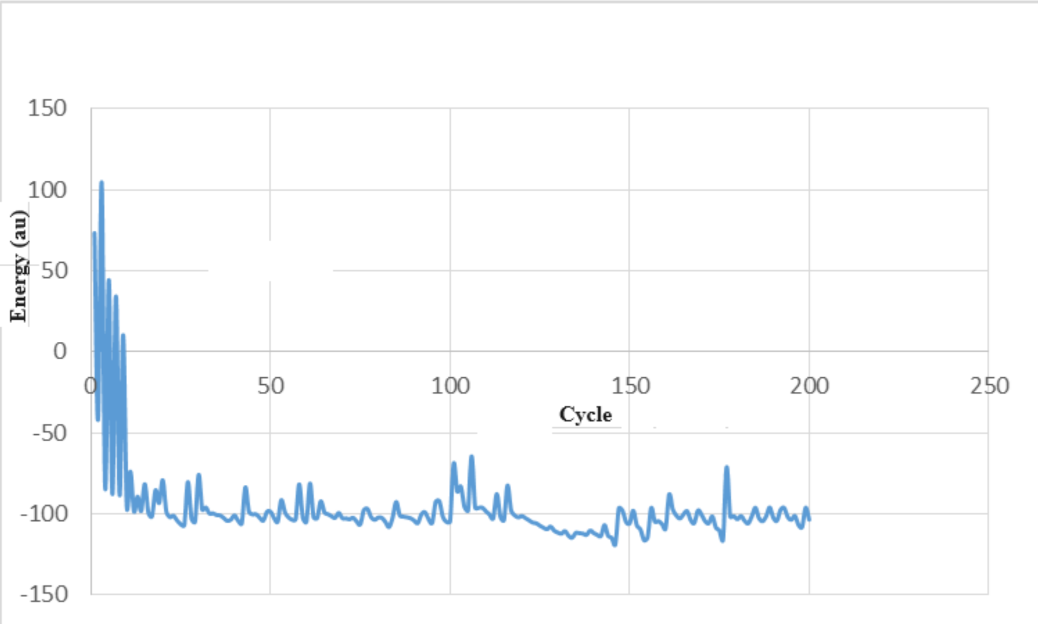

Figure 3. Geometry optimization of Compound 14 (best hit compound)

Table 3. Mulliken and ZDO atomic charges of compound 14

Atom numbers	Atoms	Mulliken atomic charges	ZDO atomic charges
1	O	-0.1382	-0.1043
2	C	-0.3580	-0.3521
3	C	-0.1395	-0.0764
4	C	0.2956	0.2700
5	C	-0.1535	-0.1404
6	C	-0.1304	-0.1282
7	C	0.4598	0.4443
8	C	0.2875	0.2692
9	C	-0.0653	-0.0635
10	C	-0.0712	-0.0623
11	C	-0.1729	-0.1471
12	C	-0.0772	-0.0799
13	C	-0.1166	-0.1085
14	C	0.3927	0.3715
15	C	0.1616	0.1477
16	C	-0.1347	-0.1254
17	C	0.1120	0.1214
18	C	0.4073	0.3413

19	C	-0.0428	-0.0261
20	C	0.2813	0.1927
21	C	0.1286	0.1293
22	C	-0.1602	-0.1411
23	C	-0.7999	-0.6806
24	C	-0.1588	-0.1378
25	C	-0.2603	-0.2806
26	C	-0.1969	-0.1691
27	C	0.5279	0.5132
28	C	-0.0518	-0.0558
29	C	-0.7126	-0.6260
30	C	0.3678	0.2746
31	C	0.5186	0.4299

Table 4. Bond length and angles of compound 14

Atoms	**Bond length (Å)**	**Atom**	**Bond angles (°)**
1 7 (O)-(C)	1.260307	1 7 3 (O)-(C)-(C)	120.000000
2 3 (C)-(C)	1.412000	1 7 17 (O)-(C)-(C)	120.000000
2 4 (C)-(C)	1.438000	3 2 4 (C)-(C)-(C)	180.000000
3 7 (C)-(C)	1.438000	2 3 7 (C)-(C)-(C)	180.000000
4 9 (C)-(C)	1.305233	2 4 9 (C)-(C)-(C)	120.000000
4 18 (C)-(C)	1.438000	2 4 18 (C)-(C)-(C)	120.000000
5 6 (C)-(C)	1.412000	3 7 17 (C)-(C)-(C)	120.000000
5 8 (C)-(C)	1.438000	9 4 18 (C)-(C)-(C)	120.000000
6 9 (C)-(C)	1.412000	4 9 6 (C)-(C)-(C)	180.000000
7 17 (C)-(C)	1.464000	6 5 8 (C)-(C)-(C)	180.000000
8 15 (C)-(C)	1.305233	5 6 9 (C)-(C)-(C)	180.000000
8 22 (C)-(C)	1.438000	5 8 15 (C)-(C)-(C)	120.000000
10 12 (C)-(C)	1.412000	5 8 22 (C)-(C)-(C)	120.000000
10 15 (C)-(C)	1.412000	7 17 25 (C)-(C)-(C)	120.000000
11 13 (C)-(C)	1.412000	7 17 28 (C)-(C)-(C)	120.000000
11 14 (C)-(C)	1.438000	15 8 22 (C)-(C)-(C)	120.000000
12 16 (C)-(C)	1.412000	8 15 10 (C)-(C)-(C)	180.000000
13 20 (C)-(C)	1.412000	12 10 15 (C)-(C)-(C)	180.000000
14 16 (C)-(C)	1.305233	10 12 16 (C)-(C)-(C)	180.000000
14 24 (C)-(C)	1.438000	13 11 14 (C)-(C)-(C)	180.000000
17 25 (C)-(C)	1.438000	11 13 20 (C)-(C)-(C)	180.000000
17 28 (C)-(C)	1.305233	11 14 16 (C)-(C)-(C)	120.000000
19 20 (C)-(C)	1.305233	11 14 24 (C)-(C)-(C)	120.000000
19 21 (C)-(C)	1.438000	12 16 14 (C)-(C)-(C)	180.000000
19 26 (C)-(C)	1.438000	13 20 19 (C)-(C)-(C)	180.000000
21 23 (C)-(C)	1.412000	16 14 24 (C)-(C)-(C)	120.000000
23 27 (C)-(C)	1.412000	25 17 28 (C)-(C)-(C)	120.000000
27 29 (C)-(C)	1.305233	20 19 21 (C)-(C)-(C)	120.000000
29 30 (C)-(C)	1.438000	20 19 26 (C)-(C)-(C)	120.000000
29 31 (C)-(C)	1.438000	21 19 26 (C)-(C)-(C)	120.000000
		19 21 23 (C)-(C)-(C)	180.000000
		21 23 27 (C)-(C)-(C)	180.000000
		23 27 29 (C)-(C)-(C)	180.000000
		27 29 30 (C)-(C)-(C)	120.000000
		27 29 31 (C)-(C)-(C)	120.000000
		30 29 31 (C)-(C)-(C)	120.000000

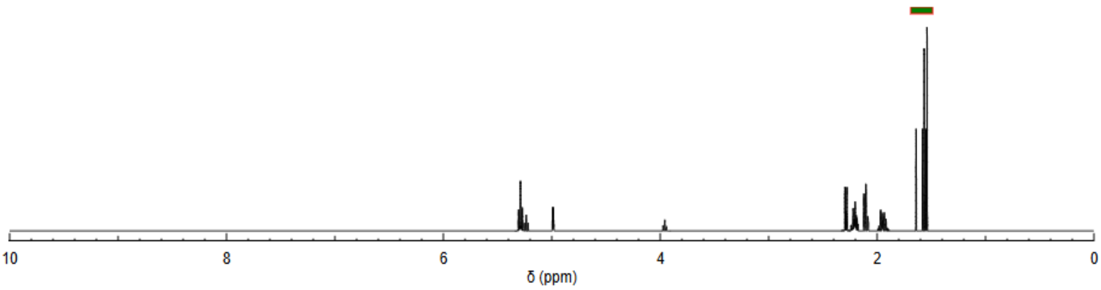

Figure 4. Simulated ^{1}H NMR of compound 14

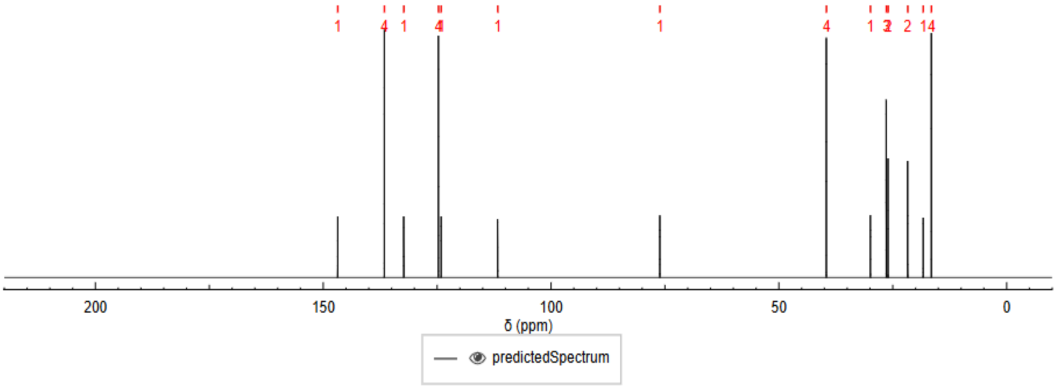

Figure 5. Simulated ^{13}C NMR of compound 14

Table 3 shows the hit compound's ZDO and Mulliken charge distributions. The higher charge densities of some carbon atoms and oxygen atom are easily noticeable. Generally speaking, the prospective locations for the electrophiles to target are those with the highest electron density [40]. There have been reports on the use of Mulliken population analysis and ZDO to investigate reaction locations [41]. The simulations demonstrated that the O and C atoms had the largest electron densities, indicating that these atoms were the active centres with the greatest capacity to bind to SARS-CoV-2 protease

Convergence was reached in order to produce the molecular geometry (Figure 3). The minimum potential energy determined by the geometry convergence function was -102.39 au. This was determined to be the optimal conformation. All of the results enabled us to identify the charged groups on the active sites that interact with the receptors. These kinds of studies are important for interactions between drugs and receptors.

In the 1H NMR spectrum (Figure 4) , the aliphatic protons (CH3, and CH2) were observed at δ 1.49-1.69 (21H, 1.54 (s), 1.54 (s), 1.55 (s), 1.56 (s), 1.57 (s), 1.58 (s), 1.64 (s)), 1.86-2.03 (4H, 1.93 (td, J = 7.5, 6.7 Hz), 1.97 (t, J = 7.5 Hz)), 2.04-2.35 (16H, 2.10 (t, J = 7.4 Hz), 2.10 (t, J = 7.4 Hz), 2.10 (t, J = 7.4 Hz), 2.20 (td, J = 7.4, 7.2 Hz), 2.21 (td, J = 7.4, 7.2 Hz), 2.21 (td, J = 7.4, 7.2 Hz), 2.29 (td, J = 7.4, 7.2 Hz), 2.29 (td, J = 7.4, 7.2 Hz)). The OH proton was observed at δ 3.96 (1H, t, J = 6.7 Hz). The vinyl protons were observed at δ 4.93-5.04 (2H, 4.98 (d, J = 1.3 Hz), 4.99 (d, J = 1.3 Hz)), 5.18-5.35 (5H, 5.24 (t, J = 7.2 Hz), 5.29 (t, J = 7.2 Hz), 5.29 (t, J = 7.2 Hz), 5.29 (t, J = 7.2 Hz), 5.29 (t, J = 7.2 Hz).

In the 3C NMR spectrum (Figure 5), the aliphatic carbons were observed at δ 16.4-16.6 (4C, 16.5 (s), 16.5 (s), 16.5 (s), 16.5 (s)), 18.3 (1C, s), 21.6-21.8 (2C, 21.7 (s), 21.7 (s)), 25.9-26.1 (2C, 26.0 (s), 26.0 (s)), 26.3-26.4 (3C, 26.4 (s), 26.4 (s), 26.4 (s)), 29.9 (1C, s), 39.5-39.6 (4C, 39.5 (s), 39.5 (s), 39.5 (s), 39.5 (s)), 76.1 (1C, s), 111.7 (1C, s). The vinyl carbons were observed at δ 124.1 (1C, s), 124.7-124.8 (4C, 124.7 (s), 124.7 (s), 124.7 (s), 124.7 (s)), 132.3 (1C, s), 136.5-136.6 (4C, 136.6 (s), 136.6 (s), 136.6 (s), 136.6 (s)), 146.8 (1C, s).

4. Conclusions

The chemical analysis revealed that the leaves of A. indica were a rich source of bioactive phytocompounds. Good binding affinity for the

NSP1 SARS-CoV-2 was shown by docking experiments. According to the molecular docking investigations, A. indica leaves may offer a good natural antiviral treatment against SARS-CoV-2. The current study demonstrated that the minimum potential energy, or -102.39 au, was the optimal conformation for the hit compound, as determined by the ArgusLab software. This conformation will increase the molecule's ability to interact with receptors, an important aspect of drug-receptor interactions.

References

[1] L. Liu, B. Mao, S. Liang, J.W. Yang, H.W. Lu, Y.H. Chai, Association between age and clinical characteristics and outcomes of COVID-19, European Respiratory Journal 55 (2020) 2001112 - 2001118.

[2] Y. Wu, C. Li, S. Xia, X. Tian, Y. Kong, Z. Wang, Identification of Human Single-Domain Antibodies against SARS-CoV-2, Cell Host Microbe 27(2020) 891–898.

[3] W.J. Guan, Z.Y. Ni, Y. Hu, W.H. Liang, C.Q. Ou, J.X. He, Clinical Characteristics of Coronavirus Disease 2019 in China, *New England.* Journal of Medicine 382 (2020) 1708–1720.

[4] X. Lu, L. Zhang, H. Du, J. Zhang, Y. Y. Li, J. Qu, SARS-CoV-2 Infection in Children, New England Journal of Medicine 382 (2020) 1663–1665.

[5] R. H. Du, L.R. Liang, C.Q. Yang, W. Wang, T.Z. Cao, M. Li, Predictors of mortality for patients with COVID-19 pneumonia caused by SARS-CoV-2: a prospective cohort study, European Respiratory Journal 55 (2020) 2000524–2000529.

[6] C. Wu, X. Chen, Y. Cai, J. Xia, X. Zhou, S. Xu, Risk Factors Associated with Acute Respiratory Distress Syndrome and Death in Patients With Coronavirus Disease 2019 Pneumonia in Wuhan, China, JAMA Internal Medicine 180 (2020) 934–943.

[7] X. Yang, Y. Yu, J. Xu, H. Shu, J. Xia, H. Liu, Clinical course and outcomes of critically ill patients with SARS-CoV-2 pneumonia in Wuhan, China: a single-centered, retrospective, observational study, Lancet Respiratory Medicine 8 (2020) 475–481.

[8] F. Zhou, T. Yu, R. Du, G. Fan, Y. Liu, Z. Liu, Clinical course and risk factors for mortality of adult inpatients with COVID-19 in Wuhan, China: a retrospective cohort study, Lancet 395 (2020) 1054–1062.

[9] T. Efferth, E. Koch, Complex interactions between Phytochemicals. The Multi-Target Therapeutic concept of Phytotherapy. Current Drug Targets 12(1) (2011) 122–132.

[10] A. Zong, H. Cao, F. Wang, Anticancer polysaccharides from natural resources: a review of recent research, Carbohydrate Polymers 90(4) (2012) 1395–1410.

[11] G. Brahmachari, Neem—an omnipotent plant: a retrospection. *ChemBioChem.* 5(4) (2004) 08–421.

[12] A.Y. Ketkar C.M. Ketkar, Various uses of neem products. In: Schmutterer H., editor. The Neem Tree. Weinheim, Germany: John Wiley & Sons, 518–525 (2004).

[13] T.R. Govindachari, G. Suresh, G. Gopalakrishnan, B. Banumathy, S. Masilamani, Identification of antifungal compounds from the seed oil of *Azadirachta indica*. Phytoparasitica. 26(2) (1998) 109–116.

[14] U. Bandyopadhyay, K. Biswas, K. and Sengupta, A. (2004). Clinical studies on the effect of Neem (*Azadirachta indica*) bark extract on gastric secretion and gastroduodenal ulcer. *Life Sciences.* 75(24) 2867–2878.

[15] A. Kher, S.C. Chaurasia, Antifungal activity of essential oils of three medical plants. Indian Drugs 15 (1997) 41–42.

[16] N. Singh, M.S. Sastry, Antimicrobial activity of Neem oil. Indian Journal of Pharmacology. 13 (1997) 102–106.

[17] P.E. Ebong, I.J. Atangwho, E.U. Eyong, G.E. Egbung, The antidiabetic efficacy of combined extracts from two continental plants: *Azadirachta indica* (A. Juss) (Neem) and *Vernonia amygdalina* (Del.) (African Bitter Leaf), The American Journal of Biochemistry and Biotechnology. 4(3) (2008) 239–244.

[18] A.J. Mordue, A. J. Nisbet, Azadirachtin from the neem tree *Azadirachta indica*: its action against insects. Anais da Sociedade Entomológica do Brasil. 29(4) (2000) 615–632.

[19] R. Paul, M. Prasad, N.K. Sah, Anticancer biology of *Azadirachta indica* L (neem): a mini review. Cancer Biology and Therapy, 12(6) (2011) 467–476.

[20] B. Sultana, F. Anwar, R. Przybylski, Antioxidant activity of phenolic components present in barks of *Azadirachta indica*, *Terminalia arjuna*, *Acacia nilotica*, and *Eugenia jambolana* Lam. trees. Food Chemistry 104(3) (2007) 1106–1114.

[21] W.C. Sarmiento, C.C. Maramba, M.I.M. Gonzales, An *in vitro* study on the antibacterial effect of neem (*Azadirachta indica*) leaf extracts on methicillin-sensitive and methicillin-resistant *Staphylococcus aureus*. Pediatric Infectious Disease **Society of** the **Philippines** *Journal* 12(1) (2011) 40–45

[22] A.A. Ahuchaogu, G.I. Ogbuehi, U. PO, I.E. Otuokere, Gas Chromatography Mass Spectrometry and Fourier transform Infrared Spectroscopy analysis of methanolic extract of Mimosa pudica L. leaves, Journals. of Drugs and Pharmaceutical Sciences 4 (1) (2020) 1- 9.

[23] K.K. Igwe, O.V. Ikpeazu, F.J. Amaku, I.E. Otuokere, I.E. (2020) Repurposing Hydroxychloroquine as a Model Drug for the Prediction of Potential SARS-CoV-2 Inhibitor: A Computational Approach, European Journal of Engineering Research and Science 5(9) (2020) 1031-1036

[24] K.K. Igwe, A.J. Madubuike, C. Ikenga, I.E. Otuokere, F.J. Amaku, Studies of the medicinal plant *Pausinystalia yohimbe* ethanol leaf extract phytocomponents by GCMS analysis. International Journal of Scientific Research and Management. 4 (2016) 4116 - 4122

[25] K.K. Igwe, P.O. Nwankwo, I.E. Otuokere, S.N. Ijioma, F.J. Amaku, GC-MS analysis of phytocomponents in the methanolic extract of *Moringa oleifera* leave, Journal of Research in Pharmaceutical science. 20 (2015) 1- 6.

[26] K.K. Igwe, A.J. Madubuike, S.C. Akomas, I.E. Otuokere, C, S. Ukwueze, Studies of the medicinal plant *Euphorbia hirta* methanol leaf extract phytocomponents by GCMS analysis , International Journal of Scientific and Technical Research in Engineering 1(4) (2016) 9-16

[27] O.V. Ikpeazu, F.J. Amaku, I.E. Otuokere, K.K Igwe, Using the Pharmacophoric features of Azithromycin to design potential SARS-CoV-2 inhibitor: A Virtual Screening and Molecular Docking Approach, European Journal of Engineering Research and Science, 5(9) (2020) 1037-1042

[28] O.V. Ikpeazu, I.E. Otuokere, K.K. Igwe, Preliminary Studies on the Secondary Metabolites of *Buchholzia coriacea* (Wonderful Kola) Seed Ethanol Extract by GC-MS Analysis, International Journal Research in Engineering and Applied Sciences **7** (2017) 17-26.

[29] O.V. Ikpeazu, I.E. Otuokere, K.K. Igwe, K.K. GC–MS Analysis of Bioactive Compounds Present in Ethanol Extract of *Combretum hispidum* (Laws) (Combretaceae) leaves, International Journal of Trend in Scientific Research and Development 4(5) (2020) 307-313.

[30] O.V. Ikpeazu, I.E. Otuokere, K.K. Igwe, Gas chromatography–mass spectrometric analysis of bioactive compounds present in ethanol extract of *Combretum hispidum* (Laws)(Combretaceae) root, Communication in Physical Sciences 5(3) (2020) 325-337.

[31] C.G. Kwekowe, E.O. Johnbull, I.E. Otuokere, Isolation and Characterization of Secondary Metabolite from the Stem Bark Extract of *Allophylus africanus* Beauv (*Sapindaceae*), Journal of Chemical Society of Nigeria. 46(2) (2021) 382–392.

[32] I.E. Otuokere, O.U. Akoh, F.C. Nwadire, C.I. Nwankwo, J.N. Egbucha, W. Chiemela, A.O. Ogbonna, GC-MS Profiling and In Silico Studies to Identify Potential SARS-CoV-2 Nonstructural Protein Inhibitors from *Psidium guajava*, African Scientific Reports 1 (2020) 161–173.

[33] I.E. Otuokere, O.U. Akoh, J.O. Echeme, F.C. Nwadire, C.I. Nwankwo, J.N. Egbucha, K. Ammasai, GC-MS Analysis and Molecular Docking Studies to Identify Potential SARS-CoV-2 Nonstructural Protein Inhibitors from *Icacina trichantha* Oliv Tubers. Trop J Nat Prod Res. 6(8) (2022) 1336-1342.

[34] I.E. Otuokere, F.J Amaku, K.K. Igwe, C.A. Bosah, Characterization of *Landolphia dulcis* Ethanol Extract by Gas Chromatography-Mass Spectrometry

Analysis, International Journal on Advances in Engineering Technology and Science, 2(4) (2016) 13-17.

[35] I.E. Otuokere, F.J. Amaku, K.K. Igwe, G.C. Chinedum, Medicinal studies on the phytochemical constituents of *Judticia carnea* by GC-MS analysis. American Journal of Food Science and Health, 2 (2016) 71-77.

[36] I.E. Otuokere, D.O. Okorie, K.K. Igwe, U.I. Matthew, Gas Chromatography-Mass Spectrometry Determination of Bioactive Phytocompounds in *Chromolaena Odorata* Leaf Extract, International Journal on Advances in Engineering Technology and Science 2 (2016) 7-11.

[37] M. A. Thompson, Planaria Software LLC, Seattle, WA. (2024) Available online:http://www.arguslab.com

[38] S. Dallakyan, A.J. Olson, Small-Molecule Library Screening by Docking with PyRx. *Methods in Molecular Biology* 1263 (2015) 243-50.

[39] S. Sivaprakash, S. Prakash, S. Mohan, S.P. Jose, Quantum chemical studies and spectroscopic investigations on 2-amino-3-methyl-5-nitropyridine by density functional theory, Heliyon 5 (2019) 1 -10.

[40] C. Gatti, The source function descriptor as a tool to extract chemical information from theoretical and experimental electron densities. Struct. Bond. 147 (2012) 193–286.

[41] A.A. Khadom, Quantum Chemical Calculations of Some Amines Corrosion Inhibitors/ Copper Alloy Interaction in Hydrochloric Acid. Journal of Materials and Environmental Sciences 8 (2017) 1153-1160.